Stability Analysis of Grid-Forming Inverter in DQ Frequency Domain

K. Oue, S. Sano, T. Kato, K. Inoue
Department of Electrical Engineering,
Doshisha University
Kyotanabe, Kyoto, 610-0321, JAPAN
E-mail: koue@mail.doshisha.ac.jp

***Abstract*— In near future, power converters will be introduced into transmission grids on a large scale due to increase of renewable energy sources. The control schemes of grid-connected inverters currently assume that there are sufficient synchronous generators (SGs) in the grid for synchronization and integration of electric power. However, when grid-connected inverters significantly outnumber SGs, there is a need for the grid-forming capability to operate the transmission grid autonomously. These inverters should generate AC voltages and are called "grid-forming" inverters. They behave as voltage sources and the cascaded PI controller has been often used. However, it is difficult to tune the control gains because of system couplings and the controller's bandwidths. This paper proposes a new controller based on the linear quadratic regulator (LQR) for voltage regulation and shows comparisons of the performances between them. It is also well known that the instability due to interactions between inverters and a grid is sometimes observed. This paper utilizes the impedance-based method in dq frame to analyze the stability of the grid-forming inverters with both the LQR and the cascaded PI controller. The stability is also investigated using eigenvalue analysis and the results are validated by numerical simulations.**

Keywords—Grid-Forming Inverter, Cascaded PI controller Linear Quadratic Regulation (LQR), Impedance-based method, eigenvalue analysis

I. INTRODUCTION

For environmental reasons, the share of electrical energy generated by distributed and renewable-energy sources, such as wind and solar power, is increasing and high-voltage direct-current (HVDC) transmission systems have been introduced. Since more renewable energy production systems and HVDC systems are interfaced to alternative grids, these applications have increased power electronic devices in the grid [1].

Nowadays, synchronous generators (SGs) dominate the electrical grid, establishing a nominal voltage amplitude and frequency that allow grid-connected inverters to inject the power to the grid and to synchronize with AC voltage at the point common coupling (PCC) by the phase locked loop (PLL) or the zero-crossing detection techniques. These inverters are called "grid-feeding" inverters.

However, as the share of grid-feeding inverters are growing rapidly, some grids will possibly be operated without synchronous devices in the future. In this case, the conventional grid-feeding inverters are not able to inject the power into the grid. For autonomous operation, the control principle of the grid-connected inverters must be dramatically changed. Inverters will need to no longer follow the grid but instead lead the grid. Grid-connected inverters based on this concept are called "grid-forming" inverters [2].

This work was supported by (MEXT/JSPS) KAKENHI Grant Number JP17K06324.

The grid-forming inverter should be able to generate an AC voltage with a given amplitude and frequency at PCC like SGs. It should be noted that a master-slave organization like that of the micro-grid is not possible in a transmission system and each inverter must operate independently only from local measurable variables. Three well-known primary controls for this autonomous operation have been proposed in the literature: the synchronverter [3], the virtual synchronous machine (VSM) [4]-[8], and the droop control [9]-[13].

Unlike inverters, SGs possess inertias and damping factors in terms of their structural properties, which introduce a slow dynamic to the frequency that is a result of rotational speed. On the other hand, the inverter's frequency is determined by its control principle, and its primary control can form virtual inertias and damping factors to grid-forming inverters. The primary control also allows inverters to synchronize to the grid without detecting the grid-phase and to share power with other generators. It is also proven that the VSM and the droop control are mathematically identical [13].

A cascaded PI controller has been applied to grid-forming inverters as an inner loop control for the voltage regulation. However, it is difficult to tune controller gains because of the system mode couplings and the controller's bandwidths. Although some methods [14]-[16] have been proposed in the literature to tune control gains, the power coupling still needs to be improved. This paper proposes a linear quadratic regulator (LQR) as an alternative controller and tunes the control gains using the participation factor [17]. It is also shown that the LQR has better transient characteristics and decoupling effects between voltage and active power than a conventional cascaded PI controller does.

It is also widely known that interactions among grid-connected inverters and grid impedance often destabilize the inverter control loop and lead instability. To analyze the stability of the circuit systems including grid-forming inverters, the impedance-based stability criterion is widely applied [18]-[21]. This paper derives the impedances of grid-forming inverters around an operating point. The stability is also analyzed based on the impedance method in case that the droop gain is varied and shows that the LQR has more stability margin than the cascaded PI controller. Since the impedance is a 2 by 2 matrix, the generalized Nyquist criterion (GNC) is applied and the eigen-loci of the transfer function should be analyzed [22]. The stability is also investigated using eigenvalue analysis and validated by numerical simulations.

This paper is organized as follow. In Section 2, the principle of the grid-forming inverter and the conventional cascaded PI controller are described. In Section 3, the proposed controller for voltage regulation based on LQR and the tuning method using the participation factor are depicted. In Section 4, the impedance of the grid-forming inverters are

978-1-7281-1842-0/19/ /$31.00 ©2019 IEEE

derived and the stability is analyzed based on the impedance-based methods are shown. Section 5 shows the conclusion.

II. THE PRINCIPLE OF THE GRID-FORMING INVERTER

A. System Modeling

Figure 1 shows the three-phase two-level grid-forming inverter connected with an AC grid through LCL filters and supplied by an ideal DC bus. In this paper, the grid is modeled as an equivalent AC voltage source. Although the conventional grid-feeding inverters synchronize to the grid by PLL and are controlled as current sources, the grid-forming inverters establish the nominal voltage amplitude with the fixed frequency. This inverter has to cope with various topologies which are modeled here by three extreme cases: (1) Standalone mode where the filtered converter is connected only to one load. (2) Autonomous mode where grid-forming inverters are connected in parallel. (3) Connection to an infinite grid modeled by a Thevenin voltage source and its equivalent impedance. The droop control is added to ensure power sharing and the synchronization.

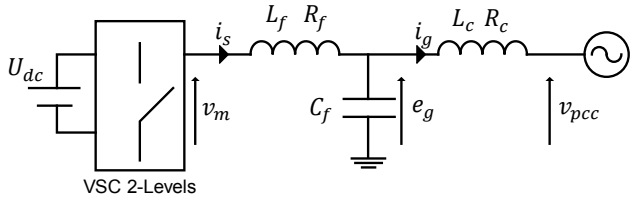

Fig. 1. Three-phase 2-levels grid-forming inverter.

Following the notations in Fig.1, the state variables are, respectively, the inverter current i_s through the inductor L_f, the voltage e_g across the filter capacitor C_f, and the current i_g through the transformer inductance L_c. U_{dc}, v_m,and v_{pcc} are, respectively, the ideal DC bus voltage, the output voltage and the grid-voltage which is transformed to the capacitor phase. The state variables are transformed in d-q frame where θ is the instantaneous phase of the capacitor voltage deduced by the droop control. The state space model for the three-phase grid-forming inverter system is as follows:

$$\begin{cases} \dot{\boldsymbol{x}}(t) = \boldsymbol{A_c x}(t) + \boldsymbol{B_c u}(t) + \boldsymbol{F_c w}(t) \\ \boldsymbol{y}(t) = \boldsymbol{C_c x}(t) \end{cases} \quad (1)$$

Where,

$$\boldsymbol{x^T} = [i_{sd} \quad i_{sq} \quad e_{gd} \quad e_{gq} \quad i_{gd} \quad i_{gq}]$$

$$\boldsymbol{u}^T = [v_{md} \quad v_{mq}]$$

$$\boldsymbol{w}^T = [v_{pccd} \quad v_{pccq}]$$

$$\boldsymbol{A_c} = \begin{bmatrix} -\frac{R_f\omega_b}{L_f} & \omega\omega_b & -\frac{\omega_b}{L_f} & 0 & 0 & 0 \\ -\omega\omega_b & -\frac{R_f\omega_b}{L_f} & 0 & -\frac{\omega_b}{L_f} & 0 & 0 \\ \frac{\omega_b}{C_f} & 0 & 0 & \omega\omega_b & -\frac{\omega_b}{C_f} & 0 \\ 0 & \frac{\omega_b}{C_f} & -\omega\omega_b & 0 & 0 & -\frac{\omega_b}{C_f} \\ 0 & 0 & \frac{\omega_b}{L_c} & 0 & -\frac{R_c\omega_b}{L_c} & \omega\omega_b \\ 0 & 0 & 0 & \frac{\omega_b}{L_c} & -\omega\omega_b & -\frac{R_c\omega_b}{L_c} \end{bmatrix}$$

$$\boldsymbol{B_c^T} = \begin{bmatrix} \frac{\omega_b}{L_f} & 0 & 0 & 0 & 0 & 0 \\ 0 & \frac{\omega_b}{L_f} & 0 & 0 & 0 & 0 \end{bmatrix}$$

$$\boldsymbol{C_c} = \begin{bmatrix} 0 & 0 & 1 & 0 & 0 & 0 \\ 0 & 0 & 0 & 1 & 0 & 0 \end{bmatrix}$$

$$\boldsymbol{F_c^T} = \begin{bmatrix} 0 & 0 & 0 & 0 & -\frac{\omega_b}{L_c} & 0 \\ 0 & 0 & 0 & 0 & 0 & -\frac{\omega_b}{L_c} \end{bmatrix}$$

The vectors $\boldsymbol{x}$ and $\boldsymbol{u}$ are the state variables and the system inputs respectively, and $\boldsymbol{w}$ is the grid-voltage considered as perturbations in this case. The output $\boldsymbol{y}$ is the voltage across the capacitor. The term of ω_b is the base value for the angular frequency in rad/s, corresponding to the rated frequency of the grid.

Figure 2 shows block diagrams of the droop control. The control is $P-\omega$ and $Q-E_g$ droop since the nature of the grid is inductive enough as $X_g \gg R_g$. The injected three-phase instantaneous active and reactive power components, and p_{mes} are q_{mes} are given by the following equations

$$p_{mes} = e_{gd}i_{gd} + e_{gq}i_{gq} \quad (2)$$

$$q_{mes} = e_{gd}i_{gq} - e_{gq}i_{gd} \quad (3)$$

To avoid power noises, a low-pass filter is added on the active and reactive power measurement, where ω_c is the cut-off frequency.

$$p = \frac{\omega_c}{\omega_c + \mathrm{s}} p_{mes} \quad (4)$$

$$q = \frac{\omega_c}{\omega_c + \mathrm{s}} q_{mes} \quad (5)$$

The droop control determines the amplitude, phase, and frequency of the capacitor voltage reference, thus grid-forming VSCs can synchronize to the grid and can share power without any detection of the grid-phase.

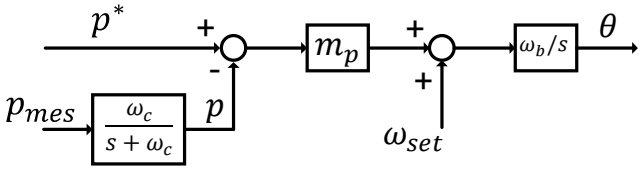

(a) P-f droop

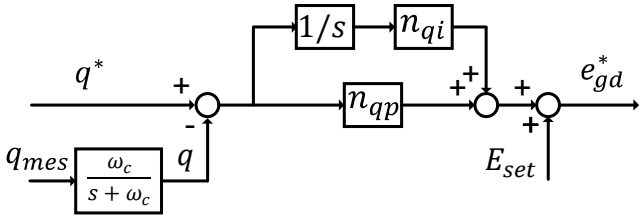

(b) Q-V droop

Fig. 2.Block diagram of droop control.

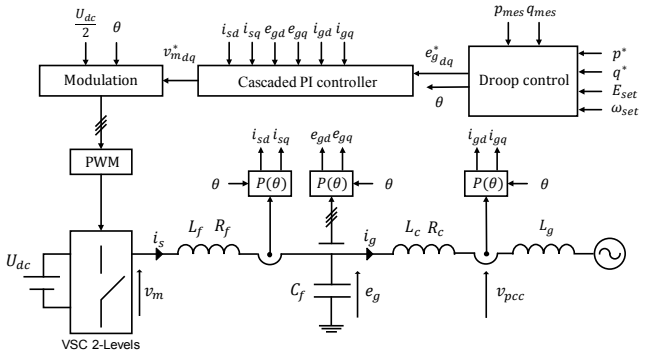

Fig. 3. Conventional grid-forming inverter control by cascaded PI controller.

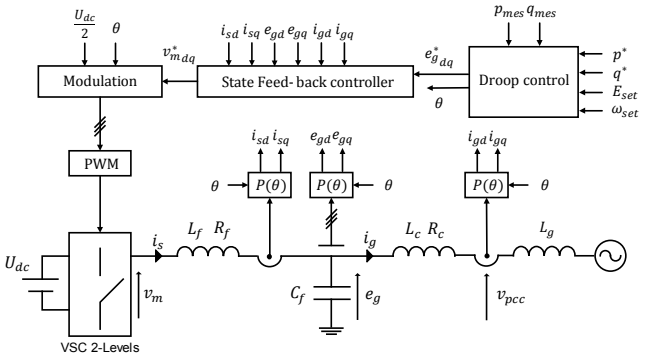

Fig. 4. Proposed grid-forming inverter control by LQR.

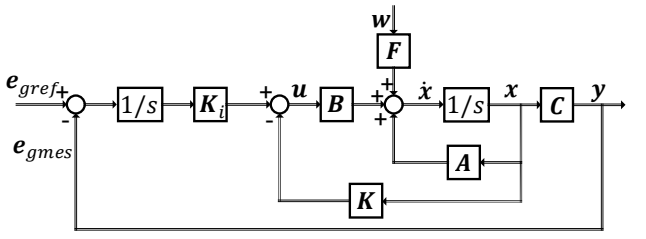

Fig. 5. Block diagram of LQR for voltage regulation.

B. Conventional cascaded PI controller

Figure 3 shows the conventional circuit diagram for a grid-forming inverter which consists of the droop and the cascaded PI controls.

The advantage of the cascaded PI controller is the ability to obtain the current reference from the voltage control so that grid-forming inverters prevent themselves from overcurrent in cased of grid-fault. However, the design of the PI controller is difficult because of the system coupling and controller's bandwidth. PI controllers in cascaded structures are independently tuned in frequency-domain by setting a faster response time for inner loop and slower one for outer loops, the system with these controller gains may be unstable in grid-connected mode.

To deal with this issue, some tuning methods have been proposed in order to ensure a stable system operation. The voltage dynamic in [14][15] is very slow with significant overshoot, whereas the results presented in [16] show a faster performances. However, the important coupling between active and reactive powers still need to be improved.

III. GRID-FORMING CONTROL BASED ON LQR

A. Design of LQR for Voltage Regulation

The whole system of the grid-forming inverter is shown in Fig. 4. This section presents a LQR controller composed of a state-feedback and an integral compensator instead of the conventional cascaded voltage and current loop controllers. An integral compensator is sufficient to control the voltage across the capacitor without any steady-state error in the synchronous rotating frame (SRF). The block diagram of the LQR system for the voltage regulation is shown in Fig. 5. $\boldsymbol{K_f}$ and $\boldsymbol{K_i}$ are the state-feedback gain and the integral compensator matrices, respectively. The vector $\boldsymbol{r}$ is defined as the voltage reference across the capacitor from the Q-V droop operation. The vector $\dot{\boldsymbol{\varepsilon}}$ is the derivative of the error between the reference and the output voltage; these are expressed in the following equations:

$$\boldsymbol{r} = [e_{gdref} \quad e_{gqref}]^T \tag{6}$$

$$\dot{\boldsymbol{\varepsilon}} = \boldsymbol{r} - \boldsymbol{y} = \boldsymbol{r} - \boldsymbol{C}\boldsymbol{x} \tag{7}$$

Augmented matrices of the controlled system are written as

$$\begin{cases} \begin{bmatrix} \dot{\boldsymbol{x}} \\ \dot{\boldsymbol{\varepsilon}} \end{bmatrix} = \begin{bmatrix} \boldsymbol{A_c} & \boldsymbol{0} \\ -\boldsymbol{C_c} & \boldsymbol{0} \end{bmatrix} \begin{bmatrix} \boldsymbol{x} \\ \boldsymbol{\varepsilon} \end{bmatrix} + \begin{bmatrix} \boldsymbol{B_c} \\ \boldsymbol{0} \end{bmatrix} \boldsymbol{u} + \begin{bmatrix} \boldsymbol{0} \\ \boldsymbol{I} \end{bmatrix} \boldsymbol{r} + \begin{bmatrix} \boldsymbol{F_c} \\ \boldsymbol{0} \end{bmatrix} \boldsymbol{w} \\ \boldsymbol{y} = [\boldsymbol{C_c} \quad \boldsymbol{0}] \begin{bmatrix} \boldsymbol{x} \\ \boldsymbol{\varepsilon} \end{bmatrix} \\ \boldsymbol{u} = -\boldsymbol{K}\boldsymbol{x} + \boldsymbol{K_I}\boldsymbol{\varepsilon} = -[\boldsymbol{K} \quad -\boldsymbol{K_I}] \begin{bmatrix} \boldsymbol{x} \\ \boldsymbol{\varepsilon} \end{bmatrix} \end{cases} \tag{8}$$

In addition, in order to utilize the LQR, augmented matrices are defined as

$$\tilde{\boldsymbol{x}} = \begin{bmatrix} \boldsymbol{x} \\ \boldsymbol{\varepsilon} \end{bmatrix} \in R^{8\times 1}, \tilde{\boldsymbol{K}} = [\boldsymbol{K} \quad -\boldsymbol{K_I}] \in R^{2\times 8}$$

$$\tilde{\boldsymbol{A}} = \begin{bmatrix} \boldsymbol{A_c} & \boldsymbol{0} \\ -\boldsymbol{C_c} & \boldsymbol{0} \end{bmatrix} \in R^{8\times 8}, \tilde{\boldsymbol{B}} = \begin{bmatrix} \boldsymbol{B_c} \\ \boldsymbol{0} \end{bmatrix}, \tilde{\boldsymbol{F}} = \begin{bmatrix} \boldsymbol{F_c} \\ \boldsymbol{0} \end{bmatrix} \in R^{8\times 2} \tag{9}$$

This controller has 16 gains in order to regulate the voltage, while the cascaded PI controller has only 8 gains, meaning that the feedback controller has a greater degree of freedom. Moreover, the coupling effect between the d- and q-axes can be taken into account when the gain matrices are determined.

The quadratic optimal regulator problem is used to determine the control gain matrix $\tilde{\boldsymbol{K}}$ so as to minimize the performance index

$$J = \int_0^\infty (\tilde{\boldsymbol{x}}^T \boldsymbol{Q} \tilde{\boldsymbol{x}} + \boldsymbol{u}^T \boldsymbol{R} \boldsymbol{u}) dt \tag{10}$$

where $\boldsymbol{Q}$ is a positive-definite (or positive-semidefinite) Hermitian or real symmetric matrix and $\boldsymbol{R}$ is a positive-definite (or positive-semidefinite) Hermitian or real symmetric matrix. Note that the first term on the right side of the equation is related to the convergence speed of each of the state variables, and the second term is related to the expenditure of the energy of the control signals. The matrices $\boldsymbol{Q}$ and $\boldsymbol{R}$ determine the relative importance of the convergence speed and the expenditure of this energy, respectively. An advantage of the quadratic optimal control method over the pole-placement method is that it provides a systematic way of computing the state-feedback control gain matrix [23].

B. *Tuning Control gains Using Participation Factors*

The servo-system for voltage regulation is determined for given the matrices $\boldsymbol{Q}$ and $\boldsymbol{R}$ values in the equations above. However, the phase of the grid-voltage and the droop control that is non-linear should be taken into account for the parameter determination. Moreover, the feedback gains should be tuned carefully to decouple the active power control from the reactive power control, which is related to voltage regulation. To consider the whole system behaviors, the eigenvalues of the system are analyzed using a small-signal state-space model around an operation point [24]. The derived small-signal model of the grid-forming inverter with LQR is as follows:

$$\Delta\dot{\boldsymbol{x}}_l(t) = \boldsymbol{A}_l\Delta\boldsymbol{x}_l(t) + \boldsymbol{B}_l\Delta\boldsymbol{u}_l(t) + \boldsymbol{F}_l\Delta\boldsymbol{w}_l(t) \qquad (11)$$

where,

$$\Delta\boldsymbol{x}_l = [\Delta\theta_s\ \Delta P\ \Delta Q\ \Delta i_{sd}\ \Delta i_{sq}\ \Delta e_{gd}\ \Delta e_{gq}\ \Delta i_{gd}\ \Delta i_{gq}\ \Delta\epsilon_{egd}\ \Delta\epsilon_{egq}\ \Delta\epsilon_q]^T$$

$$\Delta\boldsymbol{u}_l = [\Delta P_{\boldsymbol{ref}}\quad \Delta\omega_{\boldsymbol{set}}\quad \Delta e_{gdref}]^{\boldsymbol{T}}, \Delta\boldsymbol{w}_l = [\Delta v_{gd}\quad \Delta v_{gq}]^{\boldsymbol{T}}$$

The system parameters and the operating point are listed in Table 1. E_{gd}, E_{gq}, I_{gd}, and I_{gq} are values at the operating point of e_{gd}, e_{gq}, i_{gd}, and i_{gq}. θ_s can be converted to a constant value under steady-state conditions because it is defined as a voltage phase difference from the capacitor to the grid. Table 2 shows that the eigenvalues of the state transition matrix $\boldsymbol{A_l}$ when weighting matrices $\boldsymbol{Q}$ and $\boldsymbol{R}$ are identity matrices. The three eigenvalues, λ_{10-11} and λ_{12} indicate that the stability margin of this system is relatively small since they are close to the imaginary axis. The controller gains should be tuned to acquire a better stability margin.

In this paper, the participation factor is utilized to tune the control gains. The participation factor shows a sensitivity of an eigenvalue to a state variable [25]. The participation factor of mode k to a state variable j is defined as

$$\rho = \boldsymbol{q}_{kj}^T\boldsymbol{p}_{kj} \qquad (12)$$

where $\boldsymbol{q}_{kj}$ and $\boldsymbol{p}_{kj}$ are the j-th components of the left and right eigenvectors of mode k for the linearized matrix $\boldsymbol{A_l}$, respectively. The participation factors for λ_{10-11} and λ_{12} presented in Fig. 6 and Fig. 7 shows the link with ϵ_d and ϵ_q respectively. It indicates that the weighting factor Q_7 and Q_8 should be increased in order to improve the voltage dynamics. The weighing matrices are finally determined as Table 3. The eigenvalues after tuning the weighing matrices are shown in Table 4. The system has more stability margins rather than the one before the tuning.

In order to show the relevance of the proposed control, the comparison between the cascaded PI [16] and the proposed controls is investigated by MATLAB/Simulink. The voltage step response is applied to the system Eset=1.1[pu] at t=0.1s. This case is chosen in order to check the coupling between the active power and controlled voltage. The results are shown in Fig. 8. The proposed method generates a faster response without overshoot than the cascaded PI controller does. The proposed method presents a very small transient coupling effect between the active and reactive powers in contrast to the cascaded PI controller.

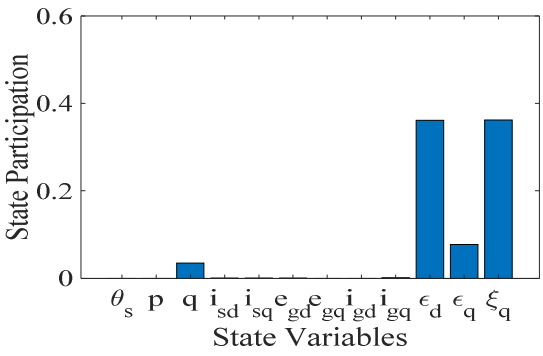

Fig. 6. State variables participation on λ_{10-11}

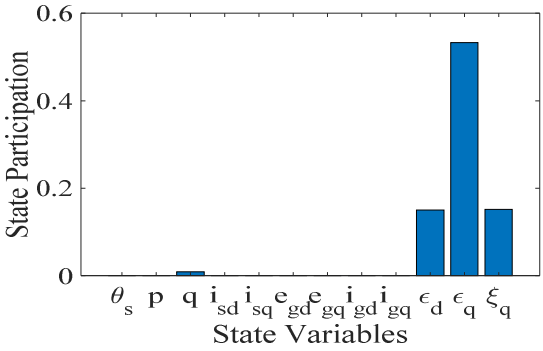

Fig. 7. State variables participation on λ_{12}

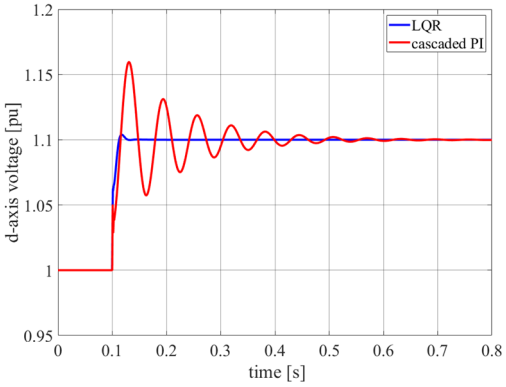

(a) d-axis voltage

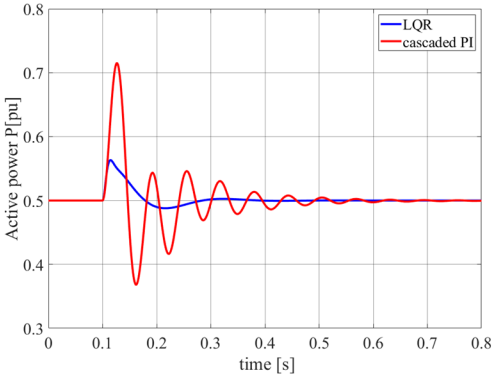

(b) Active power

Fig. 8. Proposed control performance compared to conventional one.

IV. Stability Analysys of the Grid-Forming Inverter

It has been reported that the system might be unstable when control gains are designed to be implemented.

Investigation of the stability is possible using the impedance small-signal method in dq frame. in this section, the principle of the impedance method firstly discussed and the output impedance of the grid-forming inverters with LQR is derived at an operating point. Then the stability based on the impedance method and the eigenvalue analysis is investigated and validated by the numerical simulations. Finally, the comparison the stability of the LQR to the one of the cascaded PI controller is investigated.

A. Impedance-based small-signal stability analysis

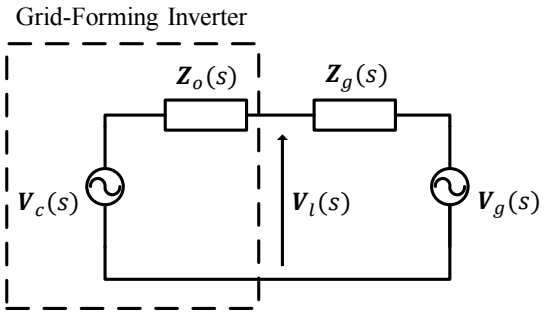

Fig. 9. Small-signal circuit of a three-phase system in dq frame.

The principle of the Impedance-based small-signal method [18] [19] is briefly reviewed to analyze the stability of a grid-forming inverter. The linearization of nonlinear circuit around the operating point is needed for deriving small-signal impedance. For a three-phase ac system, there is no fixed operating point in stationary (abc) frame. The transformation from the abc frame to the dq frame enables to exist their fixed operating point.

The system is modeled into two subsystems as shown in Fig. 9. Since the grid-forming inverter behaves as a voltage source, the inverter is expressed with the Thevenin's circuit of the output impedance $\boldsymbol{Z_o}(s)$ and the inverter control voltage $\boldsymbol{V_c}(s)$. The grid system is expressed with the Thevenin's circuit of the equivalent system voltage $\boldsymbol{V_g}(s)$ and the line impedance $\boldsymbol{Z_g}(s)$. Then the interfaced voltage $\boldsymbol{V_l}(s)$ can be written as (13), and the minor loop $\boldsymbol{L}$(s) can be defined as (14);

$$\boldsymbol{V_l}(s) = \left(\boldsymbol{I} + \boldsymbol{Z_o}(s)\boldsymbol{Z_g^{-1}}(s)\right)^{-1}(\boldsymbol{V_c}(s) - \boldsymbol{V_g}(s)) \quad (13)$$

$$\boldsymbol{L}(s) = \boldsymbol{Z_o}(s)\boldsymbol{Z_g^{-1}}(s) \quad (14)$$

Where, $\boldsymbol{I}$ is the identity matrix. The right side of the equation has a closed-loop. Applying the generalized Nyquist criterion to the minor loop $\boldsymbol{L}$(s), the system is stable if the eigenloci of $\boldsymbol{L}$(s) encircle greater than the -1, or cross the right side, when the phase is 180°[22]. It is noted that the eigenloci is the loci of the eigenvalues of the loop gain transfer function matrix parameterized as a function of frequency.

B. Stability Investigation of the Grid-Forming Inverter with LQR

In frequency-domain, the output impedance is derived from equation (6);

$$[\Delta I_{gd}(s) \quad \Delta I_{gq}(s)]^{\boldsymbol{T}} = \boldsymbol{C_l}\Delta\boldsymbol{X}(s)$$
$$= \boldsymbol{C_l}(s\boldsymbol{I} - \boldsymbol{A_l})^{-1}\boldsymbol{B_l}\Delta\boldsymbol{U}(s) + \boldsymbol{C_l}(s\boldsymbol{I} - \boldsymbol{A_l})^{-1}\boldsymbol{F_l}\Delta\boldsymbol{W_l}(s) \quad (15)$$

The second term of the right side represents the transfer function from the grid-voltages to the injected currents to the grid, and it is equivalent to the output admittance $\boldsymbol{Z_o}(s)$ around an operating point, which can be written as

$$\boldsymbol{Z_o}(s) = \begin{bmatrix} Z_{dd}(s) & Z_{dq}(s) \\ Z_{qd}(s) & Z_{qq}(s) \end{bmatrix} = (-\boldsymbol{C_l}(s\boldsymbol{I} - \boldsymbol{A_l})^{-1}\boldsymbol{F_l})^{-1} \quad (16)$$

Considering the direction of the defined current, the negative sign should be added. The line impedance $\boldsymbol{Z_g}(s)$ can be also written as;

$$\boldsymbol{Z_g}(s) = \begin{bmatrix} R_g + s\dfrac{L_g}{\omega_b} & -\omega L_g \\ \omega L_g & R_g + s\dfrac{L_g}{\omega_b} \end{bmatrix} \quad (17)$$

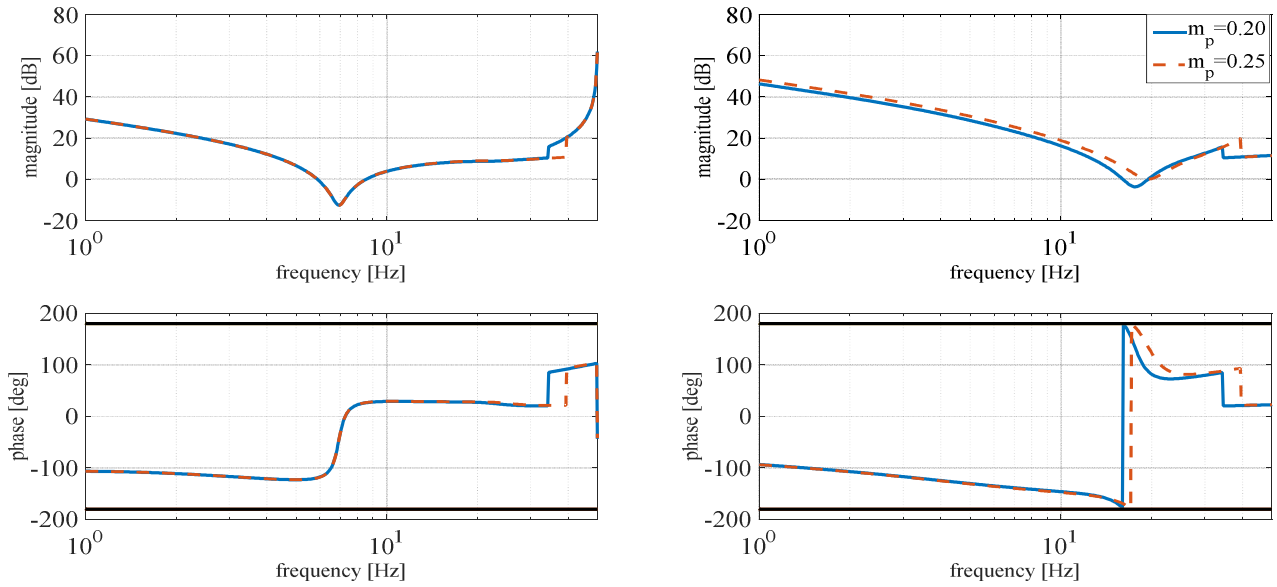

Fig. 10. Bode diagram of the eigen-loci of gain loop transfer function matrix $\boldsymbol{L}(s)$.

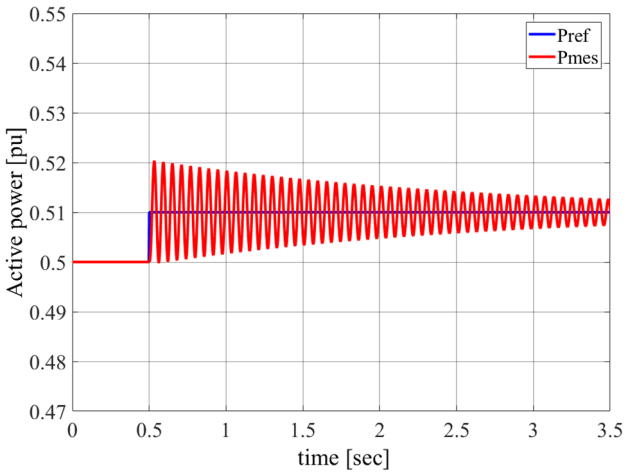

(a) m_p=0.20

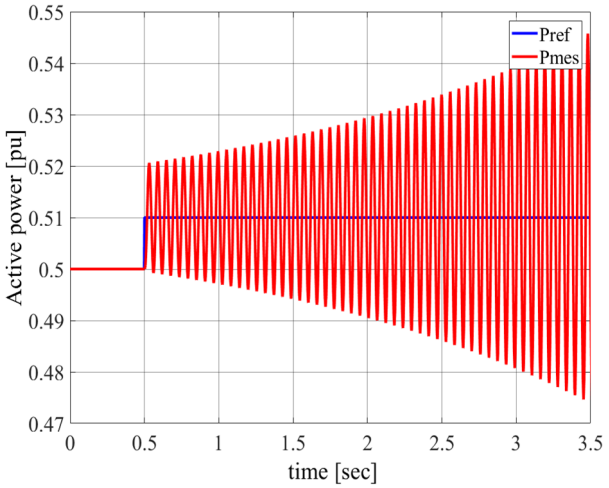

(b) m_p=0.25

Fig. 11. Simulated active power of grid-forming inverter.

The power control gain m_p is checked for the stability. Figure 10 shows the frequency characteristics of the eigenloci of the loop gain matrix $\boldsymbol{L}(s)$ when m_p=0.20 and it indicates the magnitude is -0.079 [dB] at 180° that means this is the critical point, whereas it is unstable when m_p=0.25 magnitude is 3.51 [dB] at 180°. It can be also said that an increase of the power control gain causes enlarging the output impedance gains.

The stability is also investigated using the eigenvalue analysis of the linearized matrix $\boldsymbol{A}_l$. Tables 5 and 6 show the eigenvalues of the state transition matrix $\boldsymbol{A}_l$ when the P-θ droop coefficient m_p is 0.20 and 0.21 respectively. The eigenvalues in Table 5 indicate that the system is stable, whereas the positive eigenvalues λ_{9-10} in Table 6 indicate that it is unstable. The two stability methods are mathematically identical. However, in other cases, for example, inverters are connected in parallel, the eigenvalue analysis needs considerable calculation due to the increase of the state variables. Automatic general formulation such as [26] should be utilized for analyzing large systems.

These stability analysis is validated by MATLAB/Simulink. The active power step response is applied to the system P_{ref}=0.51 [pu] at t=1 [sec]. Figure 11 (a) shows the active power is converged and the system is stable when the droop coefficient m_p =0.20, whereas the active power is diverged when m_p=0.21 in Fig. 11 (b). The stability analysis based on eigenvalues is validated with the time domain simulations.

C. Comparison the Stablity margin of LQR with Cascaded PI Controller

The output impedance of the grid-forming inverter can be derived as the same way as equation (16). The comparison of stability margins between the LQR and the cascaded PI controller is shown in Fig. 12. In this case, the stability margin is considered with the power control gain m_p fixed as 0.02. Figure 12 indicates clearly that the LQR has more stability margins rather than the cascaded PI controller.

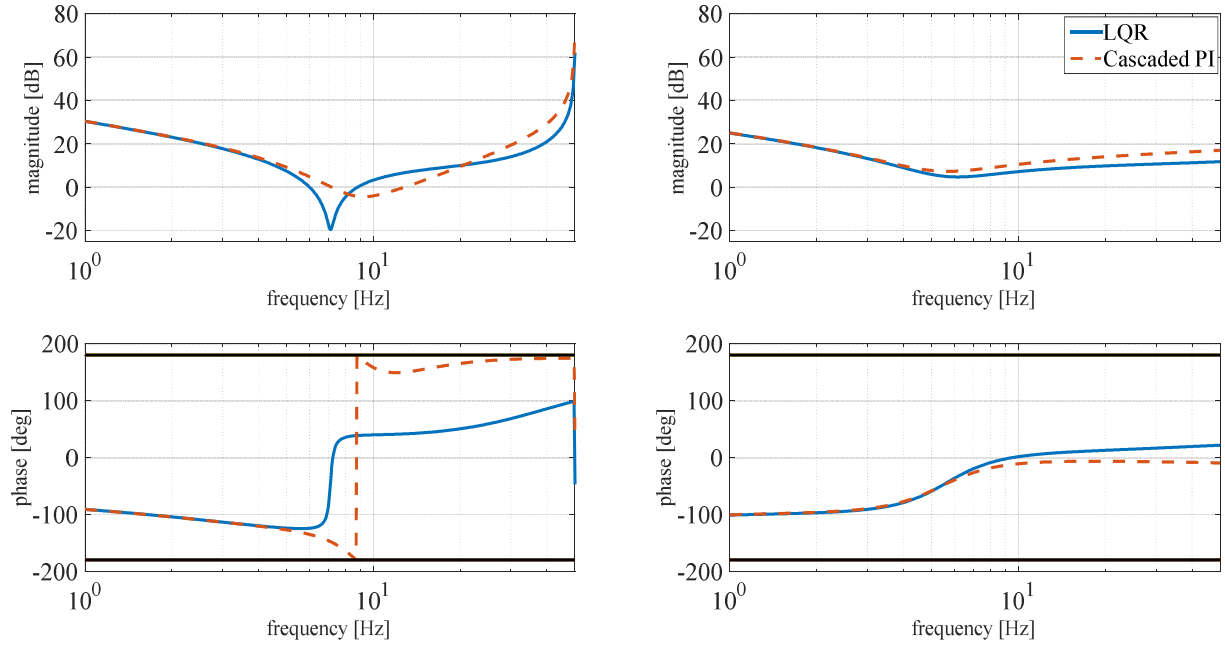

Fig. 12. Comparison of the stability margins between LQR and cascaded PI controller.

V. CONCLUSIONS

This paper proposed a new control method for the grid-forming inverter based on the LQR. Compared to the cascaded PI controller, the proposed system generates faster voltage response with lower overshoot and a very small transient coupling effect between the active and reactive powers.

The stability was also analyzed based on the impedance small-signal method in dq-frame. The output impedance $\boldsymbol{Z}_o(s)$ can be derived from the small-signal state space model and the minor loop $\boldsymbol{L}(s)$ is investigated. Although the impedance method and eigenvalue analysis get the same results since they are mathematically identical, impedance method might be preferred in case of a more complex system such as a system with multiple inverters.

The LQR has more stability margins than the cascaded PI controller. It can be said that the LQR has some potential to be applied to the grid-forming inverters.

As future subjects, experimental results are needed for the validation of the analysis and the proposed method.

Table 1. System parameters and operating point.

Parameter	Value	Parameter	Value
P	0.5 [pu]	ω_c	31.4 [rad/s]
f	50 [Hz]	R_f	0.005 [pu]
ω_{ref}	1 [pu]	L_f	0.15 [pu]
e_{gdref}	1 [pu]	R_c	0.005 [pu]
e_{gqref}	0 [pu]	L_c	0.15 [pu]
ω_b	$2\pi f$ [rad/s]	C_f	0.066 [pu]
m_p	0.02 [pu]	n_{qi}	-10 [pu]
		n_{qp}	0.1 [pu]
Operating point			
θ_s	0.316 [rad]	I_{gd}	0.5 [pu]
$\cos\theta_s$	0.95	I_{gq}	0 [pu]
$\sin\theta_s$	0.3123	V_{gd}	1 [pu]
E_{gd}	1 [pu]	V_{gq}	0 [pu]
E_{gq}	0 [pu]		

Table 2. System Eigenvalues.

$\lambda_{1-2} = -1337 \pm 4519j$	$\lambda_{3-4} = -1337 \pm 3891j$
$\lambda_{5-6} = -1137 \pm 3891j$	$\lambda_7 = -31$
$\lambda_{8-9} = -13 \pm 10j$	$\lambda_{10-11} = -0.416 \pm 3.42j$
$\lambda_{12} = -2.76$	

Table 3. Weighting matrices

$Q_1 \sim Q_6 = 1$	$Q_7, Q_8 = 10^7$	$R_1, R_2 = 1$

Table 4. System Eigenvalues after tuning

$\lambda_{1-2} = -1458 \pm 4658j$	$\lambda_{3-4} = -1375 \pm 4075j$
$\lambda_{5-6} = -1802 \pm 145j$	$\lambda_{7-8} = -162 \pm 207j$
$\lambda_{9-10} = -14 \pm 27j$	$\lambda_{10-11} = -5.19 \pm 39.1j$

Table 5. Eigenvalues of $\boldsymbol{A}_l$ when mp=0.20

$\lambda_{1-2} = -1458 \pm 4658j$	$\lambda_{3-4} = -1475 \pm 146j$
$\lambda_{5-6} = -1802 \pm 146j$	$\lambda_{7-8} = -176 \pm 194j$
$\lambda_{9-10} = -0.3 \pm 100j$	$\lambda_{11-12} = -0.570 \pm 38j$

Table 6. Eigenvalues of $\boldsymbol{A}_l$ when mp=0.25

$\lambda_{1-2} = -1458 \pm 4658j$	$\lambda_{3-4} = -1475 \pm 4075j$
$\lambda_{5-6} = -1802 \pm 146j$	$\lambda_{7-8} = -180 \pm 191j$
$\lambda_{9-10} = 3.96 \pm 112j$	$\lambda_{11-12} = -5.67 \pm 38j$

REFERENCES

[1] H. Bevrani,B. Francois,and T. Ise : *MICROGRID DYNAMICS and CONTROL* ,John Wiley & Sons, Inc, (2017)

[2] G. Denis, T. Prevost, M. Debry, F. Xavier, X. Guillaud, and A. Menze : "The Migrate project: the challenges of operating a transmission grid with only inverter-based generation. A grid-forming control improvement with transient current-limiting control", IET Renewable Power Generation, Vol.12, No.5, pp. 523-529, (2018)

[3] Q-C. Zhong and G.Weiss : "Synchronverters: inverters that mimic synchronous generators", IEEE Transactions on Industrial Electronics, Vol 58, No 4, April (2011)

[4] K. Sakimoto, Y. Miura, and T. Ise : "Characteristics of parallel operation of inverter type distributed generators operated by a virtual synchronous generator", IEEJ Transactions on Power and Energy, Vol. 133, No.2, pp.186-194 (2012)

[5] J. Alipoor, Y. Miura, andT. Ise : "Power system stabilization using virtual synchronous generator with alternatin moment of inertia", IEEE journal of emerging and selected topics in power electronics, Vol. 3, No 2, June (2015)

[6] K. Sakimoto, Y. Miura,and T. Ise : "Stabilization of a power system including inverter type distributed generators by the virtual synchronous generator", IEEJ Transactions on Power and Energy, Vol. 132, No. 4, pp.341-349 (2011)

[7] O. Mo, S. D'Acro and J-A. Suul : "Evaluation of virtual synchronous machines with dynamic or quasistationary machine models", IEEE Transactions on Industrial Electronics, Vol. 64, Issue. 7, pp. 5952-5962 (2017)

[8] M. Yu, R.Ierna, H. Urdal : "Use of and inertia-less virtual synchronous machine within future power networks with high penetrations of convertes", IEEE Power Systems Computation Conference (PSCC), pp. 1-7, (2016)

[9] G.Denis, T. Prevost, P. Panciatici, X. Kestelyn, F. Colas, and X. Guillaud : " Review on potential strategies for transmission grid operations based on power electronics interfaced voltage sources",IEEE Power & Energy Society General Meeting, pp. 1-5 (2015)

[10] J. Liu, Y. Miura, and T. Ise : " Comparison of dynamic characteristics between virtual synchronous generator and droop control in inverter-based distributed generators", IEEE Transactions on Power Electronics, Vol. 31, No. 5 (2016)

[11] V. Thomas, S. Kumaravel, and S. Ashok : "Virtual synchronous generator and its comparison to droop Control in microgrids", IEEE International Conference on Power, Instrumentation, Control and Computing (PICC),pp.1-4 (2018)

[12] R. Ofir, U. Markovic, P. Aristidou, and G. Hug : "Droop vs. Virtual Inertia: comparison from the perspective of converter operation mode",IEEE International Energy Conference (ENERGYCON),pp.1-6 (2018)

[13] S. D'Acro and J-A Suul : "Virtual synchronous machines-classification of implementations and analysis of equivalence to droop controllers for microgrids", IEEE Grenoble Conference, pp1-7 (2013)

[14] S. D'Acro, J-A Suul, and O-B Fosso : "Automatic tuning of cascaded controllers for power converters using eigenvalue parametric sensitivities", IEEE Transactions on Industry Applications, Vol. 51, No 2, pp.1743-1753 (2015)

[15] G. Denis, T. Prevost, P. Panciatici, X. Kestelyn, F.Colas, and X. Guillaud : " Improving robustness against grid stiffness,with internal control of an AC voltage-controlled VSC", IEEE Power and Energy Society General Meeting (PESGM), pp.1-5 (2016)

[16] T. Qoria, F. Gruson, F. Colas. X. Guillaud,M-S. Debry,and T. Prevost : "Tuning of cascaded controllers for robust grid-forming Voltage Source Converter", IEEE Power Systems ComputationConference (PSCC) (2018)

[17] T. Qoria, C. Li, K. Oue, F.Gruson, F.Colas, X.Guillaud, G. Denis, T. Prevost : "Tuning of AC voltage-controlled VSC based Linear Quadratic Regulation", IRSEC18, pp. 333, 2018

[18]]J. Sun : " Impedance-based stability criterion for grid-connected inverters",IEEE Transactions on Power Electronics,Vol. 26,No 11,pp.3075-3078 (2011)

[19] B. Wen, D. Dong, D, Boroyevich, R. Burgos, P. Mattavelli, and Z. Shen : "Impedance-based analysis of grid-synchronization stability for three-phase paralleled converters", IEEE Transactions on Power Electronics, Vol.31, No. 1, pp.26-38 (2016)

[20] Y. Takami, T. Kato, K. Inoue : "General-purpose computation method of a power converter for frequency characteristics: application to stability analysis of a grid inverter", IEEE Journal of Emerging and Selected Topics in Power Electronics,Vol. 5, No.4, pp.1466-1473 (2017)

[21] T. Kato, K. Inoue, and T. Sakiyama : " Stability analysis methods of a grid-connected inverter in time and frequency domains",IEEE International Power Electronics Conference (IPEC-NIIGATA2018-ECCE Asia), pp.2186-2192 (2018)

[22] Abbas Emami-Naeini and Robert L. Kosut : "The generalized Nyquist criterion and robustness margins with applications", IEEE 51th Conference on Desion and Control, (2012)

[23] K. Ogata : *MATLAB for control engineers*, Upper Saddle River, New Jersey 07458

[24] N. Pogaku, M. Prodanovic, and T-C. Green : "Modeling,analysis and testing of autonomous operation of an inverter-based microgrid", IEEE Transactions on Power Electronics, Vol. 22, No. 2, pp.613- 625 (2007)

[25] S. Danielsen, O-B Fosso,and T. Toftevaag : "Use of participation factors and parameter sensitivities in study and improvement of low-frequency stability between electrical rail vehicle and power supply", IEEE European Conference on Power Electronics and Applications, pp.1-10 (2009)

[26] A. Kaneko, K. Oue, T. Kato, and K. Inoue :"Computaion of frequency characteristics of grid inverters by general small-signal anaysis method", IEEE 20th Workshop on Control and Modeling for Power Electronics (COMPEL), Paper No. 32, (2019)